Use of remote-sensing to quantify the distribution of progradation/erosion along a forced-regressive modern coastline: driving factors and impact on the stratigraphic record

Valentin Zuchuat[1], Miquel Poyatos-Moré[2], Björn Nyberg[3,4], Rachel A. Nanson[5], Stephen Sagar[5], Leo Lymburner[5], Robbi Bishop-Taylor[5]

[1]Geological Institute, RWTH-Aachen University, Wüllnerstrasse 2, Aachen, 52062 Germany

[2]Departament de Geologia, Universitat Autònoma de Barcelona, 08193 Cerdanyola del Vallès, Spain

[3]Department of Earth Sciences, University of Bergen, Allégaten 41, 5007 Bergen, Norway

[4]Bjerknes Centre for Climate Research, Allegaten 70, 5020, Bergen, Norway.

[5]National Earth and Marine Observations Branch, Geoscience Australia, Cnr Jerrabomberra Ave and Hindmarsh Drive, Symonston ACT 2609, Australia

This version of the manuscript has been accepted for publication in *The Sedimentary Record* after the incorporation of comments and suggestions made by Andrew S. Madof and Professor Adrian Hartley (see acknowledgements).

ABSTRACT

The long-term development of ancient and modern coastal distributary distributive fluvial systems (DFSs) during periods of relative sea-level highstand or fall usually drives net-progradation of shorelines. Such systems often develop in periods of relative sea-level highstand or fall and typically record annual to millennial-scale deviations in coastal trajectories. A new continental dataset (Digital Earth Australia Coastlines: DEA Coastlines) provides an opportunity to examine such variations in coastal behaviour over annual to decadal scales (1988-2019) at local to continental spatial scales. This dataset is herein applied to the 655 km coastline fronting Australia's largest amalgamated coastal distributary distributive fluvial systems, which is situated in the epicontinental seaway of the Gulf of Carpentaria in the north of the continent. Despite the overall forced regressive conditions (i.e. progradation during relative sea-level fall), only 54% of this coastlines length net-prograded, whereas 47% was eroded. Though temporal cyclicity in progradation and erosion is evident along segments of this coast, these patterns could not be correlated with either the Southern Oscillation Index (R^2 = -0.20) or rainfall (R^2 = 0.24). Instead, short-term coastline dynamics appear to be the result of complex interactions between fluvial, wave, longshore current, and tidal processes. The high-resolution DEA Coastlines dataset highlights the diachronous, heterochronous, composite, and amalgamated nature of net-progradational stratigraphic strata that can develop in shallow-marine environments where hinge-points between prograding and retrograding

coastal segments are dynamic features that migrate with time. Our conclusions show that shorelines display granular temporal and spatial deviations in coastal trajectory, with contemporaneous progradation and erosion occurring over 1-100 km length scales. This is significantly more heterogeneity than previously envisaged, thereby suggesting the need for updating models of coastal systems.

Key words: Forced regression, DEA Coastlines, Gulf of Carpentaria, progradation, erosion, bounding surface

INTRODUCTION

Sedimentary coastal systems are shaped by temporally-variable cycles of erosion and deposition that contribute to the incompleteness and heterogeneity in the stratigraphic record. Such erosion-deposition cycles are recorded in the landscape by the development of beach ridges and cheniers (Semeniuk, 1995; Tamura, 2012). Annual to multi-decadal events and cycles (e.g. the El Niño–Southern Oscillation (ENSO), the Pacific Decadal Oscillation (PDO), the Atlantic Multi-decadal Oscillation (AMO), Dansgaard-Oeschger (DO), or DO-like events (see Boulila et al., 2022)) likely contribute to such gaps, owing to: (i) the complex nature of these cycles (both for cause(s) and consequences); (ii) the along-strike variability of coastal dynamics; (iii) the highly-variable preservation potential of sediments; and (iv) the increasing loss of time resolution and calibration with age. Detailed studies of modern analogue coastal sedimentary systems that examine these processes can be used to inform longer-term analyses for a range of end-users (e.g. basin analyses, policy makers).

Coastline trajectories reflect the ratio between the rates of accommodation creation (A) and sediment supply (S) (Helland-Hansen and Martinsen, 1996): progradation occurs when $A<S$, with $A>0$ (i.e. during a normal regression), or when $A<0$ (i.e. during a period of relative sea-level fall: forced regression). However, the study of modern marginal-marine systems has demonstrated that the spatial and temporal distribution of sediment supplied and the combination of oceanic processes play important roles in the along-strike and dip variability in coastal dynamics (Nanson et al., 2013; Nyberg and Howell, 2016; Lane et al., 2017). Waves and tides can remobilise and redistribute sediments along- and off-shore, and these changes vary by temporal and spatial fluctuations in the frequency and intensity of wave, tide and fluvial processes (see discussion in Overeem et al., 2022). Further, the amount of sediment being deposited or eroded near the shore is not linearly correlated to the intensity of extreme events (Guisado-Pintado and Jackson, 2019). These extreme events can, each time they occur, offset decadal coastline-trajectory trends (Harley et al., 2022). Both the non-linear relationship between the volume of eroded/deposited sediments and extreme-events intensity, as well as the offset-potential associated with each events make interpretation of the preserved signals more complicated. Consequently, coastline trajectories can vary markedly along individual isochrones, which can be simultaneously prograding and retrograding either side of hinges or pivot points (Madof et al., 2016; Nanson et al., 2022).

We utilise a multi-decadal remote-sensing dataset (Digital Earth Australia's Coastlines (DEA Coastlines; Bishop et al., 2021) to investigate the complexity of annual to decadal coastal dynamics fronting Australia's largest, amalgamated, Holocene, forced-regressive, Distributive Fluvial Systems (DFSs) and their deposits that have accumulated on the eastern shore of the Gulf of Carpentaria (GoC; Fig. 1). High-frequency cyclic erosion and depositional styles and Holocene rates of progradation have been well-documented for these systems (Rhodes, 1982; Jones et al., 1993, 2003; Nanson et al., 2013; Massey et al., 2014; Lane et al., 2017; Porritt et al., 2020). The relatively limited anthropogenic modification of these systems over the last 200 years (Nanson et al., 2013) provides a natural laboratory to investigate the roles of various autogenic and allogenic controls on coastal change, and to frame considerations of preservation potential in the stratigraphic record.

GEOLOGICAL SETTING

The Gulf of Carpentaria (GoC) is an epicontinental seaway in Northern Australia, which connected to the Arafura and Coral Seas to the north and is characterized by a low gradient and bathymetry (< 70m; Torgersen et al., 1983). Drainage catchments initiate in the Great Dividing Range to the east and have created four large and amalgamated DFSs (Gilbert, Staaten, Mitchell, and Coleman). The deltas of these DFSs are mixed-influence (wave, tide, and fluvial), with peak fluvial discharge during the monsoonal season (December-March; Australian Bureau of Meteorology (BoM)). The combination of relative sea-level fall attributed to hydrostatic uplift (Chappell et al., 1982), low-gradient bathymetry, and increased sedimentation during the past 4 ka has led to between ca. 0.84 km/kyr to ca. 3 km/kyr of forced-regressive shoreline progradation, which varies both in time and space (Nanson et al., 2013; Lane et al., 2017; Porritt et al., 2020).

Tides in the GoC are diurnal (Neil et al., 2021) and mesotidal, with maximum range of 4 m near Karumba (Hopey and Smithers, 2010; Figure 1a). Significant wave height (*sensu* Munk and Arthur, 1951) over the past 30 years extracted from nine control points along the studied coastline (Wavewatch III®) reaches ca. 30 cm, although storm wave heights are expected to be much greater (3.5 m peak height in the monsoon; Nanson et al., 2013). Sediment flux data is sparse between rivers. The Gilbert River (Fig. 1) has been estimated to supply ca 1 Mm^3/yr since the start of the Holocene (Porritt et al., 2020), and models of the Mitchell River predicted 2.9 Mt/yr of silt and clay reaching the GoC (Rustomji et al., 2010).

METHODS

The DEA Coastlines dataset contains yearly point series linked to lines that show the dominant median annual position of the coastline at 0 m annual mean sea level for each year between 1988-2019 (Bishop-Taylor et al., 2021). Datapoints were derived every 30 m along the whole of Australia's coastline from the Digital Earth Australia archive of Landsat satellite images (Dhu et al., 2017). These were constrained by pixel-based tidal modelling to avoid artefacts associated with varied tidal stages at the time satellite imagery was acquired, in order to generate a smooth coastline every year for the whole of Australia (Bishop-Taylor et al., 2021). The final dataset was then successfully validated by comparing it to independently measured coastline positions around Australia (Bishop-Taylor et al., 2021). It also contains average rates of progradation for every data point along the coastline (positive rates of progradation = actual progradation; negative rates of progradation = erosion).

Yearly data along the targeted segment between Karumba and Aurukun were directly exported from the main DEA Coastlines dataset (coordinates: 140.82801°E/-17.46528°S to 141.69620°E/-13.26780°S; detail python script in Appendix A). The overall coastal progradation between 1988-2019 was plotted from this dataset after each yearly sub-dataset was averaged along a 100 m rolling window (Fig. 1A). The average rates of progradation between 1988-2019 (Fig. 1B) were plotted using a modified ShowYourStripes script originally developed by Maximilian Nöthe (modified script in Appendix B). The difference in position between each year was calculated for each data point from the 100-m-averaged sub-dataset (Fig. 1C), and colour-coded in red if the coastline retreated between two subsequent years, or in blue if the coastline prograded (script used to generate plot available in Appendix C).

Wave-energy data and direction of coastal progradation were collected using the from Wavewatch III®, a hindcast average wave directions for the past 30 years (NOAA, 2022). Precipitations and Southern Oscillation Index (SOI) data were downloaded from the Australian Bureau of Meteorology (BoM, 2022). The total precipitation in each river catchment along the GoC was calculated based on the delineations of Nyberg et al. (2018).

RESULTS

Coastal behaviour (progradation vs erosion)

Despite the overall forced regressive conditions of the GoC within the last 6000 years (Nanson et al., 2013; Lane et al., 2017; Sloss et al., 2018; Porritt et al., 2020), the shorter-term behaviour of the studied coastal segment is heavily heterogeneous, both in terms of spatial distribution and magnitude of change. Only 54.23 % of the coastline length experienced a net progradation between 1988-2019, whereas 47.77 % was eroded. A majority of the total coastline movement over the 32 years of observations was between -100 and +100 m (87%); exceptional progradation reached a maximum of 372 m, whereas maximum observed erosion was 761 m (Fig. 1A). The town of Pormpuraaw north of the Mitchell delta separates the progradation-erosion results in two domains: i) the southern domain from Karumba to Pormpuraaw, and ii) the northern domain, from Prompuraaw to Aukurum (Fig. 1A). The southern domain is characterised by greater progradation-erosion amplitudes (average progradation of 49.67 m and average erosion of 54.48 m) than the northern domain between 1988-2019, where the amplitude between progradation and erosion values are smaller (average progradation 13.85 m of and average erosion of 26.29 m). Additionally, coastlines near active river mouths in the southern domain have been very mobile between 1988-2019. For example, the coastline on the southern side of the Mitchell River mouth has moved over a distance of ca. 1 km between 1988-2019. This high degree of mobility rapidly decreases away from the river mouth towards beaches and cheniers. About 46 % of the studied coastline experienced average rates of progradation between -2 and 2 m/yr (Fig. 1B), extraordinarily reaching maximum rates of -60 and 34 m/yr. When averaged for the entire studied coastal segment between 1988-2019, 4.29 m of the coastal sediments were eroded between 1988-2019. This means that the average rate of progradation for the entire studied coastline is -0.14 m/yr. The results do not provide, however, a volumetric indication of how much sediment was eroded or deposited between 1988-2019. Figure 1C displays the yearly coastal erosional or progradational behaviour along the studied section of the GoC, which can be regarded as a Wheeler diagram (Wheeler, 1958; 1964). This yearly coastal behaviour diagram (as well as the raw data) shows that only very few laterally-restricted (< 100 m) segments along the studied coastline have exceptionally experienced a continuous progradation or erosion between 1988-2019 (e.g. 15.91952°S, 141.38092°E). Some places might have experienced a near-continuous progradation or erosion (e.g. 13.49470°S, 141.56499°E), but this multi-decadal trend is nearly always offset by at least one or two off-trend years. This yearly coastal behaviour diagram as well as the values of yearly coastal behaviour averaged for the whole studied coastline (Fig. 1D) display a poorly-defined four to six years cyclical alternation of periods dominated by coastal progradation versus periods dominated by coastal erosion.

Coastal progradation controls

Total precipitation is used here a proxy for sediment being supplied to the coastline: increased precipitation would liberate more onshore sediment, thereby creating net progradation (or vice versa). Total precipitation over all the catchments feeding rivers that reach the studied coastline also shows oscillating multi-year phases of high and low precipitation. Compared to the yearly-averaged Southern Oscillation Index (SOI), precipitation is characterised by a R^2 value of 0.54, in line with reported trends for Australia (Wu and Leonard, 2019). It seems, however, that the cyclical pattern observed in the average coastal behaviour is poorly correlated to both the total precipitation and the SOI, with R^2 values of 0.24 and -0.20 respectively (Fig. 1D).

Wave direction data show that most of the studied coastline is impacted by two sets of waves propagating towards the NNE and SE/SSE (Fig. 1A, 1E; Supplementary Material A), reaching a maximum energy level of 1.557 J/m^2, while 75 % of the significant wave height was between 0.2 and 0.45 m at nine of the offshore data points. Between 1988-2019, 34 major storms and tropical cyclones have affected the area, including the tropical cyclones Barry and Ethel (1996), Abigail (2001), Grant (2011), Oswald (2013) and Nora (2018) (BoM; complete list in Appendix D). Despite the scarcity of available data, some of these events were associated with heavy rainfall, storm surges, high tides and waves (note: the nearest tide and wave gauges is near Weipa, north of the studied coastal segment). For instance, Ethel generated a storm surge of 1.18 m, with a significant wave height and a peak wave height of 3.76 m and 6.69 m respectively, while Nora generated a 1.2 m storm surge (BoM, 2022). The storm surge that accompanied Barry destroyed a fishermen' camp, built 4 m above the high-water mark, between the mouths of the Gilbert and the Staaten rivers, flooding up to 7 km inland (BoM, 2022).

Precipitation, however, is not distributed equally across the hinterland of the studied coastline (Fig. 2B), with more precipitation per surface unit in the northern than in the southern domain. R^2 statistical test results (Fig. 2D) show that both the average and the sum of coastal behaviour per coastal segment associated with each catchment or group of catchments (normalised or not) are independent of: (1) the size of each catchment (R^2_{av} = 0.11; R^2_{sum} = 0.12; $R^2_{av\_norm}$ = 0.13; $R^2_{sum\_norm}$ = 0.14); (2) the total amount of precipitation within each catchment normalised by the size of each catchment (R^2 = 0.07); and (3) the length of the coastal segment associated with each catchment or group of catchments ($R^2_{av\_norm}$ = 0.20; $R^2_{sum\_norm}$ = 0.15; Fig. 2B-D).

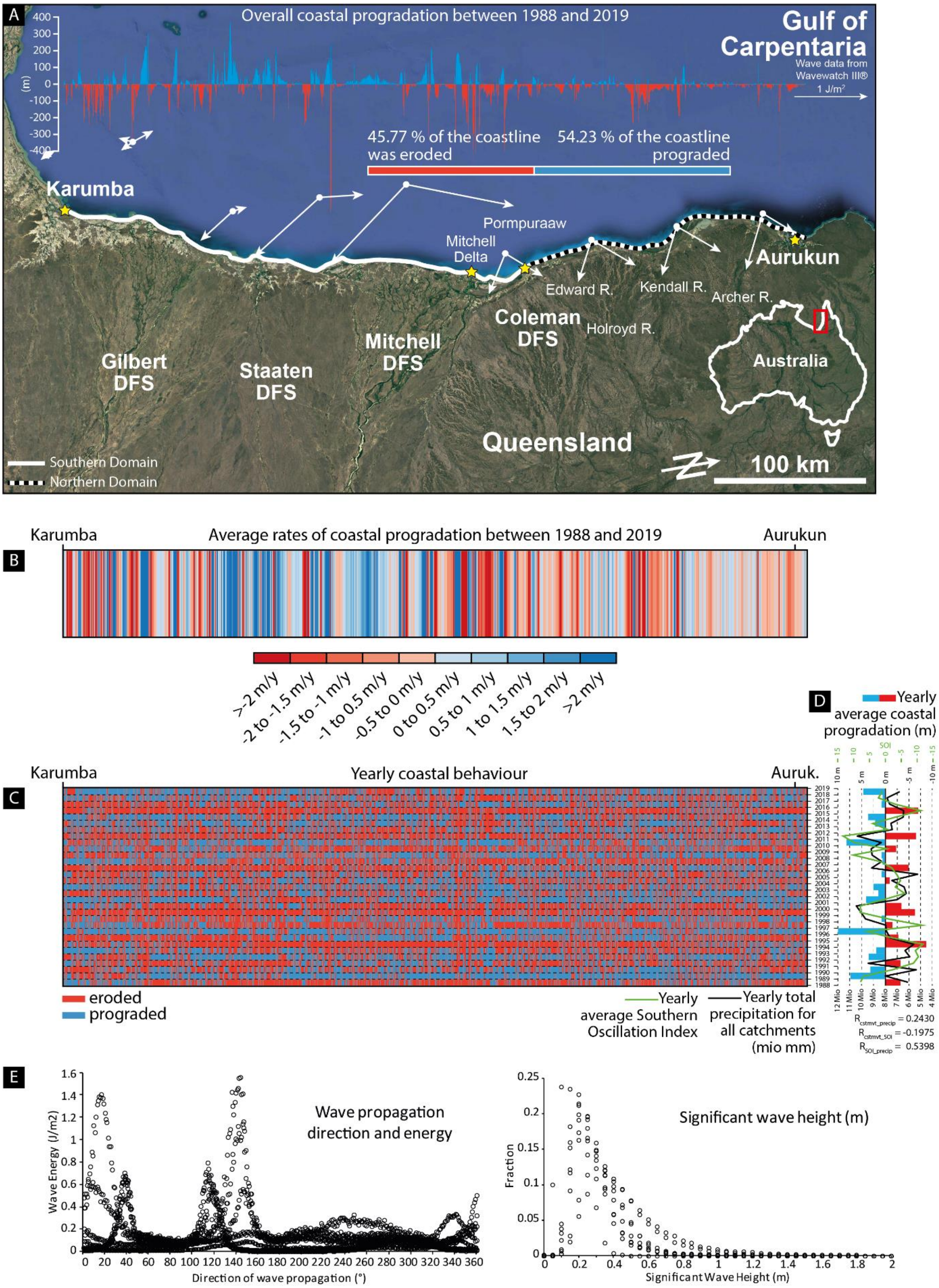

Fig. 1 – (A) Spatial distribution of coastline progradation (in m) along the Queensland margin of the Gulf of Carpentaria where Gilbert, Staaten, Mitchell, and Coleman DFSs reach the sea. The 45.77 % erosion VS 54.23 % progradation graph summarizes the entire coast. Continuous white line along the coast: Southern Domain; black-white dashed line along the coast: Northern Domain. White arrows indicate wave direction and their length is scaled to 1 J/m2 (satellite imagery ©Google Earth). (B) average rates of coastline progradation between 1988-2019 (m/y). (C) Yearly coastal behaviour plots. (D) Yearly total precipitations for all catchments (Mio mm) plotted against the yearly average coastal behaviour (m), and the yearly average Southern Oscillation Index (SOI), with Pearson test results comparing the three parameters (precipitation and SOI data from BoM). (E) Wave direction of propagation, energy, and significant wave height (data extracted from Wavewatch III® using the Global Wave and Tide Data app developed by Jaap Nienhuis; see Fig. 1A for location of datapoints).

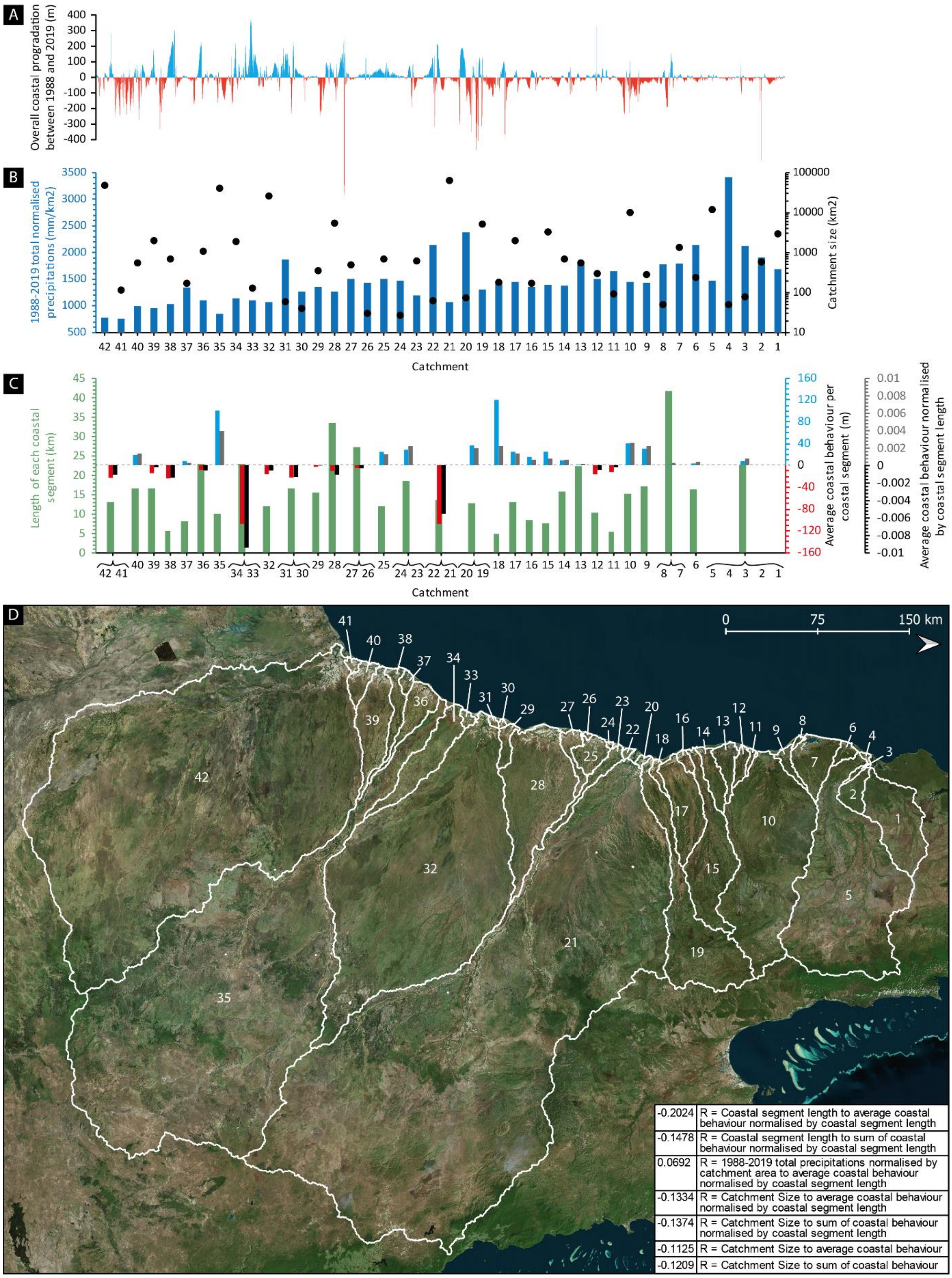

Fig. 2 – Plot series comparing (A) the coastline progradation (in m) along the studied coastline to (B) the total 1988-2019 precipitations of each catchment normalised by the surface of each catchment (blue bars). Black dots = actual size of each catchment. (C) Length of coastal segment associated with each catchment or group of catchments (green bars), average coastal behaviour per coastal segment of each catchment or group of catchments (red-blue bars), and average coastal behaviour per coastal segment of each catchment or group of catchments normalised by the length of each coastal segment (light red-blue bars. (D) Outline of each river catchment, with Pearson test results comparing the different parameters (satellite imagery Bing based on TomTom, Earthstar Geographics SIO imagery (2022)).

DRIVING FACTORS AND PRESERVATION OF THE SIGNAL IN THE ROCK RECORD

DFSs represent the dominant landform in present day continental sedimentary basins (Hartley et al., 2010; Weissmann et al., 2010), and are very often associated with a long-term prograding trend as the system grows from high sediment input (e.g. Fisher et al., 2007; Davidson et al., 2013; Weissmann et al., 2013). This long-term prograding trend has been recognised along the GoC (Nanson et al., 2013; Lane et al., 2017; Sloss et al., 2018; Porritt et al., 2020). Our results, however, highlight that the short-term trend between 1988-2019 along the studied coastline does not follow the overall regressive trend, as nearly half the studied coastline experienced erosion/transgression during the studied time period. Nevertheless, and although most of the sediment is supplied by different rivers reaching the GoC, the behaviour of the total studied coastline does not correlate to the precipitation-proxied river discharge to the shoreline. Rather than sediment supply alone, the dynamics of the coastline between 1988-2019 seem to have been more dependent on the sum of fluvial, wave action, longshore currents, and tidal processes along the studied system, but given a lack of detailed historical wave, longshore current, and tidal data in the Gulf of Carpentaria, these factors could not be studied in further detail. Furthermore, the i) nature of the substrate, as well as the spatial distribution of cohesive clays (and other cohesive biogenic substances) along the coastline (e.g. Lichtman, et al., 2018; Wu et al., 2022), ii) the change in gradient through time and space associated with varying rates of relative sea-level change (Rodriguez et al., 2001; Ruggiero et al., 2016), and iii) the type, rates of change, and degree of vegetation near the shoreline (e.g. Thampanya et al., 2006; Konlechner et al., 2019) could certainly enhance or dampen the overall mobility of the coastline (how much the coastline migrates) and the rates at which the coastline moves (how fast the coastline migrates). Nevertheless, DFSs are affected by continuous lateral channel migration or frequent avulsions at a kyr timescale (Porritt et al., 2020; Colombera and Mountney, 2022) depending on grainsize and sediment load (Cazanacli et al., 2022), none of which occurred within the time frame covered by the DEA Coastline dataset. Such avulsions would influence the spatial distribution of wave, tidal, and fluvial processes along the coastline, as well as diverting the sediment supply. Thus, even though shallow-marine processes actively redistributed the sediments along the studied coastline and were the driving factors responsible its short-term dynamics, the influence of fluvial processes might still be substantial, but more inferred or deferred rather than direct. As a result, the quantification of each of the role/influence is blurred by the amalgamation of different timescales, resulting in a potential over- or under-interpretation of the sedimentary processes that acted at the time of deposition.

Results have shown how dynamic a segment of the coastline of the GoC has been between 1988-2019, regarding both spatial and temporal dimensions. Despite the lack of volumetric quantification of the erosion and progradation phases which limits our ability to answer precisely “how much of this signal is preserved in the rock record”, these results highlight that the highly-variable and unpredictable short-term dynamics of these systems, and allow the following question to be raised: is there a minimum spatial and temporal scale below which progradational or retrogradational trends cannot be differentiated? In other words, at what moment does time sufficiently amalgamate through space for a general, basin-wide trend to emerge, or when does the overall sum of local progradation (or erosion) reach threshold points that allow general trends to be identified? This dataset covers the last 30 years, which in geological terms is virtually instantaneous, and the coastline behaviour suggests it cannot be characterised as undergoing a forced regression at this time scale. Indeed, the average rate of coastal progradation between 1988-2019 is -0.14 m/yr. Although being spatially extremely variable, this average rate of coastal progradation suggests a short-term average reversal ~~or~~ of the coastal behaviour when compared to the longer-term Holocene progradational rates which range between 0.84 m/yr to ca. 3.0 m/yr, and accelerated to 3.8 m/yr in the last 400 years (Nanson et al., 2013; Porritt et al., 2020). The exact explanation as to why this 1988-2019 average rate of coastal progradation is so different from the longer-term Holocene progradational rates is beyond the scope of this manuscript. Also, the resulting time-stratigraphy is completely different from one location to another along the studied coastline segment (Fig. 3). As a consequence of this, stratigraphic surfaces bounding coastal strata developed in different years are heavily diachronous (through time) and heterochronous (at different times), composite, and amalgamated (i.e. regressive surfaces, flooding surfaces; Fig. 3). This is not a new concept in stratigraphy (e.g. Kyrkjebø et al., 2004; Holbrook and Bhattacharya, 2012; Miall, 2016; Gani, 2017; Zuchuat et al., 2019), but it is first time it has ever been clearly documented in real time.

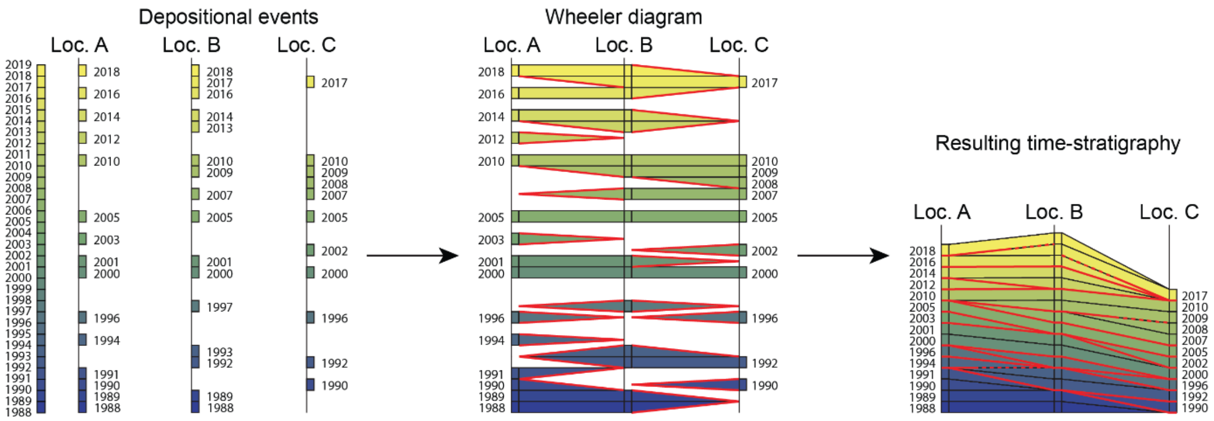

Fig. 3 –Pseudo-logs illustrating the various depositional events occurring at each of the locations, as well as the resulting time stratigraphy and the degree of amalgamation of stratigraphic surfaces (see Fig. 1C for locations).

In addition to the diachronous and heterochronous nature of these surfaces, our results show that hinges between areas of progradation and retrogradation are dynamic features that migrate spatially depending on the temporal scale considered (Fig. 4A). The consequence of the spatial migration of these hinges is that, on each side of a “time-averaged” hinge (i.e. the type of hinge usually available in the sedimentary record), the preserved stratigraphy can display characteristics of short-term transgression and regression ~~on each side of the hinge~~, even though the longer-term trend on one side of the hinge is progradational and the other one is transgressive. Because sequence stratigraphic units are defined “a relatively conformable succession of genetically related strata bounded by unconformities and their correlative conformities” (Mitchum, 1977; Van wagoner et al., 1987), these migrating hinges will further encumber the often-oversimplified lateral correlation of these stratigraphic surfaces. Furthermore, the resulting stratigraphy associated with migrating hinges will only rarely be complete, even though the longer-term trend considered is associated with a constant progradation of the coastline (Fig. 4B). Despite the increased complexity, implementing this concept of migrating hinges can help to refine the interpretation of the architecture of the preserved strata, as well as the distribution of heterogeneities in the stratigraphy, and therefore increase the robustness of basin models.

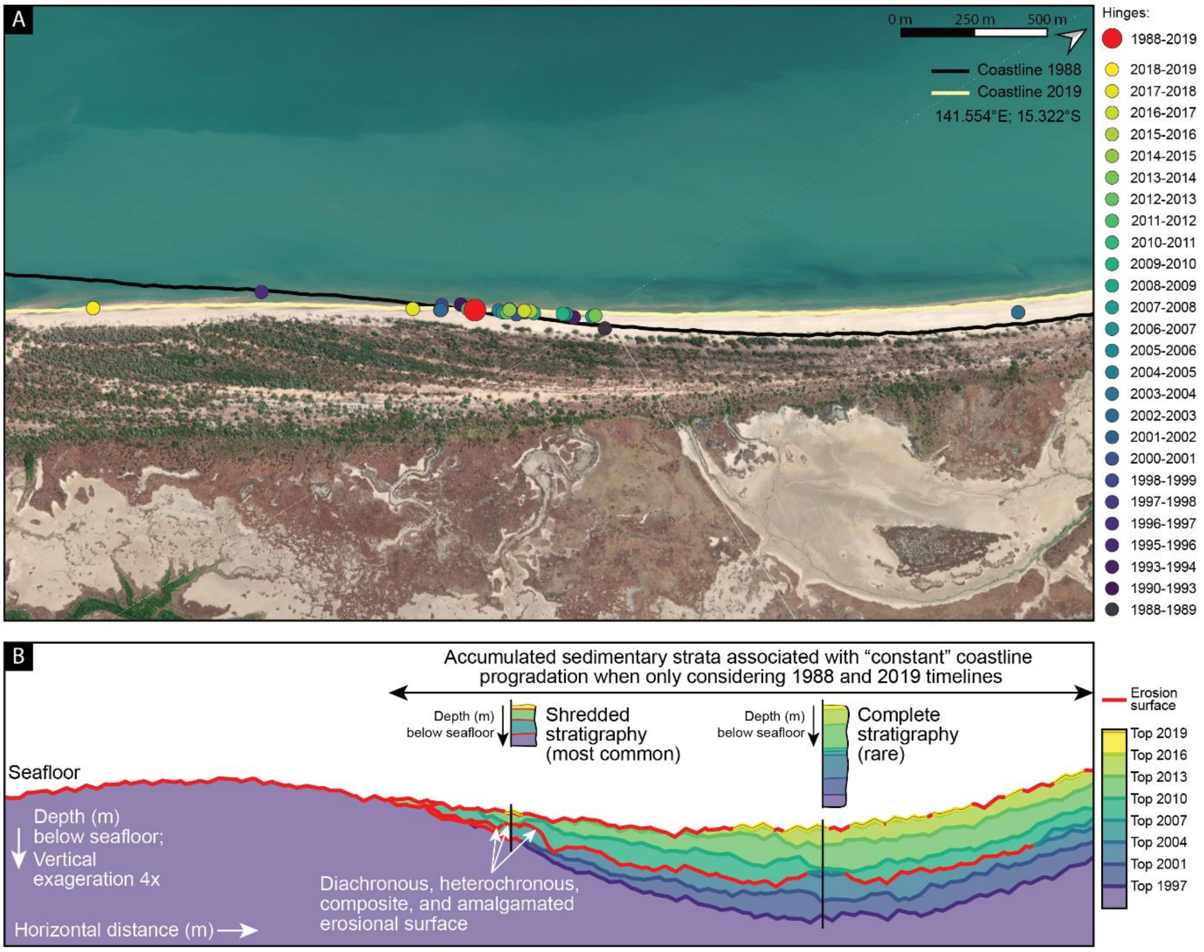

Fig. 4 – (A) Detailed photograph of a segment of the studied coastline indicating the position of the hinges between zones of progradation and zones of erosion through time (satellite imagery Bing based on TomTom, Earthstar Geographics SIO imagery (2022)). (B) Conceptual, along-strike vertical cross-section, illustrating the complex preserved sedimentary architecture resulting from the spatio-temporal migration of hinges in a zone that is characterised by a longer-term “constant” coastline progradation. Note that the artificial thickness of each yearly package was derived from the raw progradation distance from the DEA Coastlines dataset.

CONCLUSIONS

The yearly movements of a 655km segment of the Queensland coastline along the Gulf of Carpentaria between Karumba and Aurukun were calculated using the Digital Earth Australia Coastlines data between 1988-2019. Results show that:

- The mean average rate of coastline progradation for the study area is -0.14 m/yr using the DEA Coastlines dataset. This average rate encompasses considerable spatial and temporal variability.
- Only 54.23 % of the coastline length underwent net-progradation between 1988-2019, whereas 47.77 % was subject to net-erosion, with most of coastline prograding or retreating by 100 m, with progradation rates mostly between -2 and 2 m/yr.
- Multi-year overall progradation-erosion cycles correlate poorly to both the Southern Oscillation Index and the total precipitation in catchments recorded over the study area (used a proxy for sediment supply). The dynamics of the studied coastline between 1988-2019 seem to have therefore been more dependent on the sum of fluvial, wave action, longshore currents, and tidal processes rather than sediment supply alone.
- Hinges between areas of progradation and retrogradation are dynamic features that migrate depending on the temporal scale considered. The intricate nature of stratigraphic surfaces developed on each side of hinges in such dynamic shallow-marine environments makes their lateral correlation difficult. The documented short-term coastal behaviour will encumber longer-term basin reconstructions and sequence stratigraphic analysis, because of the amalgamation of various timescales occurring along the system. Nevertheless, a better understanding of the temporal and spatial complexity and the dynamics of net-progradational coastal systems and the implementation of this complexity in geomodels will help increase their robustness.

ACKNOWLEDGMENTS

Nyberg is funded by AkerBP ASA under the Fluvial Architectural Element Characterization project. The authors would like to acknowledge Dr Jenn Pickering, editor of *The Sedimentary Record*, as well as Dr Andrew S. Madof and Professor Adrian Hartley for their fruitful comments that have improved the quality of this manuscript.

DATA AVAILABILITY

All the Digital Earth Australia Coastlines data are publicly and freely available at: https://cmi.ga.gov.au/data-products/dea/581/dea-coastlines#access. The python codes used for Appendix A: total progradation between 1988-2019 (Fig. 1A); Appendix B: progradation rates (Fig. 1B); and Appendix C: Wheeler diagram (Fig. 1D) are all available on GitHub: https://github.com/Strativa l/QueenslandCoastlineGoC. The table of tropical cyclones that affected the area between 1988-2019 (Appendix D) are attached to the online version of this article. Precipitation and tropical cyclone data are both downloaded from on the BoM website: http://www.bom.gov.au/jsp/ncc/climate_averages/decadal-rainfall/index.jsp?maptype=6&period=7605&product=totals#maps and http://www.bom.gov.au/cyclone/tropical-cyclone-knowledge-centre/history/past-tropical-cyclones/. Wavewatch III® data and information available at: https://polar.ncep.noaa.gov/waves/hindcasts/

CONFLICT OF INTEREST

The authors declare no conflict of interests.

REFERENCES

Bishop-Taylor, R., Nanson, R., Sagar, S., & Lymburner, L. (2021). Mapping Australia's dynamic coastline at mean sea level using three decades of Landsat imagery. Remote Sensing of Environment, 267, 112734.

Boulila, S., Galbrun, B., Gardin, S., & Pellenard, P. (2022). A Jurassic record encodes an analogous Dansgaard–Oeschger climate periodicity. Scientific Reports, 12(1), 1-16.

Catuneanu, O. (2019). Scale in sequence stratigraphy. Marine and Petroleum Geology, 106, 128-159.

Cazanacli, D., Paola, C., & Singh, A. (2022). Sediment Load and Grain Size Controls on Channel Migration Patterns in Experimental Deltas. Journal of Geophysical Research: Earth Surface, e2021JF006402.

Chappell, J., Rhodes, E. G., Thom, B. G., & Wallensky, E. (1982). Hydro-isostasy and the sea-level isobase of 5500 BP in north Queensland, Australia. Marine Geology, 49(1-2), 81-90.

Colombera, L., & Mountney, N. P. (2022). Scale dependency in quantifications of the avulsion frequency of coastal rivers. Earth-Science Reviews, 104043.

Davidson, S. K., Hartley, A. J., Weissmann, G. S., Nichols, G. J., & Scuderi, L. A. (2013). Geomorphic elements on modern distributive fluvial systems. Geomorphology, 180, 82-95.

Dhu, T., Dunn, B., Lewis, B., Lymburner, L., Mueller, N., Telfer, E., Lewis, A., McIntyre, A., Minchin, S. and Phillips, C., 2017. Digital earth Australia–unlocking new value from earth observation data. Big Earth Data, 1(1-2), pp.64-74.

Fisher, J. A., Nichols, G. J., & Waltham, D. A. (2007). Unconfined flow deposits in distal sectors of fluvial distributary systems: examples from the Miocene Luna and Huesca Systems, northern Spain. Sedimentary Geology, 195(1-2), 55-73.

Gani, M. R. (2017). Mismatch between time surface and stratal surface in stratigraphy. Journal of Sedimentary Research, 87(11), 1226-1234.

Guisado-Pintado, E., & Jackson, D.W. (2019). Coastal impact from high-energy events and the importance of concurrent forcing parameters: The cases of storm Ophelia (2017) and storm Hector (2018) in NW Ireland. Frontiers in Earth Science, 7, 1-18.

Harley, M. D., Masselink, G., Ruiz de Alegría-Arzaburu, A., Valiente, N. G., & Scott, T. (2022). Single extreme storm sequence can offset decades of shoreline retreat projected to result from sea-level rise. Communications Earth & Environment, 3(1), 1-11.

Hartley, A. J., Weissmann, G. S., Nichols, G. J., & Warwick, G. L. (2010). Large distributive fluvial systems: characteristics, distribution, and controls on development. Journal of Sedimentary Research, 80(2), 167-183.

Helland-Hansen, W., & Martinsen, O. J. (1996). Shoreline trajectories and sequences; description of variable depositional-dip scenarios. Journal of Sedimentary Research, 66(4), 670-688.

Holbrook, J. M., & Bhattacharya, J. P. (2012). Reappraisal of the sequence boundary in time and space: case and considerations for an SU (subaerial unconformity) that is not a sediment bypass surface, a time barrier, or an unconformity. Earth-Science Reviews, 113(3-4), 271-302.

Hopley, D., & Smithers, S. (2010). Queensland. In Bird, C.F. (Ed.), Encyclopedia of the World's Coastal Landforms. Springer Science+Business Media, Dodrecht, 1255-1266.

Jones, B.G., Martin, G.R. & Senapati, N. (1993). Riverine—tidal interactions in the monsoonal Gilbert River fandelta, northern Australia. Sedimentary Geology, 83(3-4), 319-337.

Jones, B.G., Woodroffe, C.D., & Martin, G.R. (2003). Deltas in the Gulf of Carpentaria, Australia: forms, processes and products. In Sidi, F.H., Nummedal, D., Imbert, P. Darman, H. & Posamentier, H.W. (Eds), Tropical Deltas of Southeast Asia- Sedimentology, Stratigraphy and Petroleum Geology. SEPM (Society for Sedimentary Geology) Special Publication, 76, 21-43.

Kyrkjebø, R., Gabrielsen, R. H., & Faleide, J. I. (2004). Unconformities related to the Jurassic–Cretaceous synrift–post-rift transition of the northern North Sea. Journal of the Geological Society, 161(1), 1-17.

Konlechner, T. M., Kennedy, D. M., Cousens, R. D., & Woods, J. L. (2019). Patterns of early-colonising species on eroding to prograding coasts; implications for foredune plant communities on retreating coastlines. Geomorphology, 327, 404-416.

Lane, T. I., Nanson, R. A., Vakarelov, B. K., Ainsworth, R. B., & Dashtgard, S. E. (2017). Evolution and architectural styles of a forced-regressive Holocene delta and megafan, Mitchell River, Gulf of Carpentaria, Australia. In Hampson, G. J., Reynolds, A. D., Kostic, B., & Wells, M. R. (Eds), Sedimentology of Paralic Reservoirs: Recent Advances. Geological Society, London, Special Publications, 444(1), 305-334.

Lichtman, I. D., Baas, J. H., Amoudry, L. O., Thorne, P. D., Malarkey, J., Hope, J. A., ... & Ye, L. (2018). Bedform migration in a mixed sand and cohesive clay intertidal environment and implications for bed material transport predictions. Geomorphology, 315, 17-32.

Madof, A. S., Harris, A. D., & Connell, S. D. (2016). Nearshore along-strike variability: Is the concept of the systems tract unhinged?. Geology, 44(4), 315-318.

Massey, T.A., Fernie, A.J., Ainsworth, R.B., Nanson, R.A. and Vakarelov, B.K. (2014). Detailed mapping, three-dimensional modelling and upscaling of a mixed-influence delta system, Mitchell River delta, Gulf of Carpentaria, Australia. In Martinius, A.W., Howell, J.A., & Good, T.R. (Eds), Sediment-Body Geometry and Heterogeneity: Analogue Studies for Modelling the Subsurface. Geological Society, London, Special Publications, 387(1), 135-151.

Miall, A. D. (2016). The valuation of unconformities. Earth-Science Reviews, 163, 22-71.

Mitchum, R.M. (1977). Seismic stratigraphy and global changes of sea level, part 1: Glossary of terms used in seismic stratigraphy. In Payton C.E. (Ed.), Seismic stratigraphy—applications to hydrocarbon exploration. American Association Petroleum Geologists Memoir, 26, 205-212.

Munk, W. H., & Arthur, R. S. (1951). Forecasting ocean waves. In Malone, T.F. (Ed.), Compendium of Meteorology. American Meteorological Society, Boston, MA, 1082-1089.

Nanson, R. A., Vakarelov, B. K., Ainsworth, R. B., Williams, F. M., & Price, D. M. (2013). Evolution of a Holocene, mixed-process, forced regressive shoreline: the Mitchell River delta, Queensland, Australia. Marine Geology, 339, 22-43.

Nanson, R., Bishop-Taylor, R., Sagar, S., & Lymburner, L. (2022). Geomorphic insights into Australia's coastal change using a national dataset derived from the multi-decadal Landsat archive. Estuarine, Coastal and Shelf Science, 265, 107712.

Neill, S. P., Hemer, M., Robins, P. E., Griffiths, A., Furnish, A., & Angeloudis, A. (2021). Tidal range resource of Australia. Renewable Energy, 170, 683-692.

Nyberg, B. (2019). Source to Sink Database. https://doi.org/10.7910/DVN/ETH8VN

Nyberg, B., & Howell, J. A. (2016). Global distribution of modern shallow marine shorelines. Implications for exploration and reservoir analogue studies. Marine and Petroleum Geology, 71, 83-104.

Nyberg, B., Gawthorpe, R. L., & Helland-Hansen, W. (2018). The distribution of rivers to terrestrial sinks: Implications for sediment routing systems. Geomorphology, 316, 1-23.

Overeem, I., Nienhuis, J. H., & Piliouras, A. (2022). Ice-dominated Arctic deltas. Nature Reviews Earth & Environment, 3(4), 225-240.

Porritt, E. L., Jones, B. G., Price, D. M., & Carvalho, R. C. (2020). Holocene delta progradation into an epeiric sea in northeastern Australia. Marine Geology, 422, 106114.

Rhodes, E.G., 1982. Depositional model for a chenier plain, Gulf of Carpentaria, Australia. Sedimentology, 29(2), pp.201-221.

Rodriguez, A. B., Fassell, M. L., & Anderson, J. B. (2001). Variations in shoreface progradation and ravinement along the Texas coast, Gulf of Mexico. Sedimentology, 48(4), 837-853.

Ruggiero, P., Kaminsky, G. M., Gelfenbaum, G., & Cohn, N. (2016). Morphodynamics of prograding beaches: A synthesis of seasonal-to century-scale observations of the Columbia River littoral cell. Marine Geology, 376, 51-68.

Rustomji, P., Shellberg, J., Brooks, A., Spencer, J., & Caitcheon, G. (2010). A catchment sediment and nutrient budget for the Mitchell River, Queensland. Tropical Rivers and Coastal Knowledge (TRACK), 1-119.

Semeniuk, V. (1995). The Holocene record of climatic, eustatic and tectonic events along the coastal zone of Western Australia—a review. Journal of Coastal Research, 247-259.

Sloss, C. R., Nothdurft, L., Hua, Q., O'Connor, S. G., Moss, P. T., Rosendahl, D., ... & Ulm, S. (2018). Holocene sea-level change and coastal landscape evolution in the southern Gulf of Carpentaria, Australia. The Holocene, 28(9), 1411-1430.

Tamura, T. (2012). Beach ridges and prograded beach deposits as palaeoenvironment records. Earth-Science Reviews, 114(3-4), 279-297.

Thampanya, U., Vermaat, J. E., Sinsakul, S., & Panapitukkul, N. (2006). Coastal erosion and mangrove progradation of Southern Thailand. Estuarine, coastal and shelf science, 68(1-2), 75-85.

Torgersen, T., Hutchinson, M. F., Searle, D. E., & Nix, H. A. (1983). General bathymetry of the Gulf of Carpentaria and the Quaternary physiography of Lake Carpentaria. Palaeogeography, Palaeoclimatology, Palaeoecology, 41(3-4), 207-225.

Van Wagoner, J.C., Mitchum, R.M., Posamentier, H.W. & Vail, P.R. (1987). Seismic stratigraphy interpretation using sequence stratigraphy; part 2, key definitions of sequence stratigraphy. In Bally, A.W. (Ed.), Atlas of Seismic Stratigraphy 1, American Association Petroleum Geologists, Studies in Geology, 27, 11-14.

Weissmann, G. S., Hartley, A. J., Nichols, G. J., Scuderi, L. A., Olson, M., Buehler, H., & Banteah, R. (2010). Fluvial form in modern continental sedimentary basins: distributive fluvial systems. Geology, 38(1), 39-42.

Weissmann, G.S., Hartley, A.J., Scuderi, L.A., Nichols, G.J., Davidson, S.K., Own, A., Atchley, S.C., Bhattacharyya, P., Chakraborty, T., Ghosh, P., Nordt, L.C., Michel, L., & Tabor, N.J. (2013). Prograding distributive fluvial systems–geomorphic models and ancient examples. In Driese, S.G. & Nordt, L.C. (Eds), New Frontiers in Paleopedology and Terrestrial Paleoclimatology: Paleosols and Soil Surface Analog Systems, SEPM Society for Sedimentary Geology, Tulsa, OK, USA, 131-147.

Wheeler, H.E. (1958). Time Stratigraphy. American Association Petroleum Geologists Bulletin, 42, 1047-1063.

Wheeler, H.E. (1964). Baselevel, Lithosphere Surface, and Time-Stratigraphy. Geological Society of America Bulletin, 75(7), 599-610

Wu, W., & Leonard, M. (2019). Impact of ENSO on dependence between extreme rainfall and storm surge. Environmental Research Letters, 14(12), 124043.

Wu, X., Fernandez, R., Baas, J. H., Malarkey, J., & Parsons, D. R. (2022). Discontinuity in Equilibrium Wave-Current Ripple Size and Shape and Deep Cleaning Associated With Cohesive Sand-Clay Beds. Journal of Geophysical Research: Earth Surface, 127(9), e2022JF006771.

Zuchuat, V., Midtkandal, I., Poyatos-Moré, M., Da Costa, S., Brooks, H. L., Halvorsen, K., ... & Braathen, A. (2019). Composite and diachronous stratigraphic surfaces in low-gradient, transitional settings: The J-3 “unconformity” and the Curtis Formation, east-central Utah, USA. Journal of Sedimentary research, 89(11), 1075-1095.